NUMERICAL MODEL VALIDATION USING PHYSICAL MODEL DATA

Yafei Jia[1] and Sam, S.Y. Wang[2]

ABSTRACT

With the advances in numerical methods, three dimensional models for free surface turbulent flows have been accepted as a tool in the hydraulic research and applied to studies of flow field, sediment transport and pollutant transport for engineering projects. Because of the complexity of the flow physics, numerical model simulations are only approximations to the real physical processes. Comparing with the physical model data, *Physical Validation*, is the only way to exam weather or not the predictions of a numerical model can reflect the true physics concerned.

In this paper, several cases of validating a three-dimensional free-surface turbulence flow model, CCHE3D, using physical model data, such as free overfall flow, curved channel flows and flow over a submerged weir, are presented. These cases indicate that dynamic pressures, free surface algorithms and sophisticated turbulence closure schemes, etc. are essential to predicting correct physics in turbulent flows.

INTRODUCTION

In order to make sure the computational results of a particular numerical model is reliable and consistent with the flow physics under investigation, capabilities of this numerical model for predicting realistic physical processes and phenomena have to be confirmed before the model is accepted and applied to simulating real world problems. A numerical model is a complex system of equations wrapped with boundary conditions, it is not guaranteed to have these capabilities even it has been proven to be mathematically correct, unless they have been validated with physical model data. Since flow conditions in physical experiments are controlled and the physical processes are observed with minimal uncertainty, the agreements of the numerical model results and measurement indicate the consistency of the model and the true physics. In addition, a numerical model for general flow simulation should have many capabilities, validation tests using different physical model experiments should be carried out to evaluate each one of them.

Since free surface distribution, turbulence characteristics and dynamic pressure are important flow features to hydraulic engineering, the test cases selected in this paper will show validation of these capabilities. The numerical model selected, CCHE3D, is a three dimensional free surface turbulent flow model, developed at the National Center for Computational Hydroscience and

[1] Research Associate Professor, National Center for Computational Hydroscience & Engineering, The University of Mississippi, Carrier Hall Room 102, P.O. Box 1848, University, MS 38677-1848, USA. Phone: 1-662-915-7783 Fax: 1-662-915-7796 Email: jia@ncche.olemiss.edu
[2] F.A.P. Barnard Distinguished Professor & Director, National Center for Computational Hydroscience & Engineering, The University of Mississippi, Carrier Hall Room 102, P.O. Box 1848, University, MS 38677-1848, USA. Phone: 1-662-915-6562 Fax: 1-662-915-7796 Email: wang@ncche.olemiss.edu

Engineering. These cases have been selected for numerical model validation by the ASCE (American Society of Civil Engineers) Task Committee (Wang, et al. 2005).

Free overfall

Free overfall flows have been observed at nick point or head-cut of natural river channels and at manmade in-stream structures such as weir or drop structures. Numerous laboratory experiments have been conducted to study this phenomenon. Free over-falls have at least three special features, i.e. the flows turn from subcritical to supercritical near the brink of the channel, they are bounded by strongly curved free surfaces and the vertical pressure distribution near the free fall is non-hydrostatic. The results obtained from laboratory experiments by Rajaratanam and Muralidar (1968) are chosen as a validation test case for free surface flow models. It provides developers of 3D numerical models with a simple way to determine the model's capabilities in predicting non-hydrostatic pressure field in the supercritical free surface flow and in handling two free surface boundaries.

The free overfall flow physical model experiments performed by Rajaratanm and Muralidhar (1968) are sketched in Figure1, and the flow condition selected for this test case is listed in the Table 1.

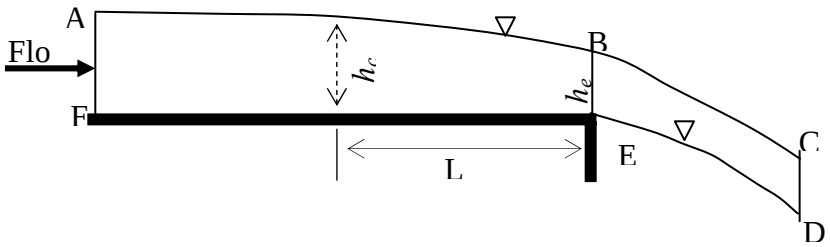

Figure1. Sketch of the free overfall flow experiment, (*FE>L*)

Among many data sets collected and published in their paper, the most comprehensive set, Test 1A, was selected for numerical simulation. The experiment was conducted in a rectangular flume, 0.457m wide and 6.1m long, with a flat and horizontal bed. The approaching flow from upstream is subcrictial, it reaches the critical condition before the brink. *L* is the so called "Length of Overfall", the length between the critical flow point and the brink. The flow depth at the brink (h_e) is actually less than the critical depth (h_c). Velocity and shear stress were measured by a calibrated pitch probe and a Prandtl tube with an external diameter of 3mm. Since the flow is symmetric to the center line, its variation in transverse direction can be neglected by simulating just the flow in the central vertical plan. As a result, one only needs to specify at the inlet the unit discharge *q* for the simulation.

Table 1. Flow condition of test case 1A, Rajaratanm and Muralidhar (1968)

Run No.	Bed slope, *So*	Unit discharge *q* (m^2/s)	Critical depth, h_c (m)	End depth, h_e (m)	Length of overfall Z(m)
1A	0.0	0.143	0.128	0.0945	0.286

Boundary conditions for each portion of the flow boundary were specified. Namely, (1) the atmospheric pressure (p_a) should be specified along the surface *AC, DE*, and the end section *CD*; (2)

hydrostatic pressure should be prescribed along the upstream inlet section *AF*; and (3) over the solid bed surface, *EF*, $\partial^2 p/\partial z^2 = 0$ is prescribed, which approximates the pressure variation very close to the bed as linear. If one sets the simulation channel longer than the length of the free fall, *L* (Figure1), one can simply prescribe subcritical flow boundary conditions at the inlet *AF*, supercritical flow boundary condition would have to be used otherwise. The dynamic pressure at the brink is non-zero, but it vanishes at the section *CD* (Rouse 1936, Strelkoffand Moayeri, 1970). The length of the free fall part is long enough to ensure that the atmospheric pressure can be applied at *CD*. The vertical location of this section and its water depth depend on the final profile of the overfall flow which are therefore unknown prior to the beginning of the simulation. In the simulation example, this section is located along the trajectory of the flow, and depth of this section is assumed to be equal to the adjacent upstream section ($\partial(\eta_t - \eta_l)/\partial s = 0$). *x* and *z* are horizontal and vertical coordinates, respectively, *s* denotes the direction along the flow, η is the free surface with subscript *t* and *l* indicating the top and lower free surface, respectively.

Due to the fact that the initial locations of the two free-surface boundaries are unknown, analytic solutions (Marchi, 1993) were used as guessed initial conditions for faster convergence. A numerical grid was generated to discretize the computational domain, which has finer resolution near the brink and near the lower boundary of bed and lower free surface. The two free surfaces are moving boundaries and they have to be located dynamically, the actual computational domain or the locations of the free-surface boundaries were modified in each time step until the steady state flow is reached. At this time, the steady state solutions of velocity and pressure fields were obtained. The numerically simulated results were compared to the experimental measurements of Rajarathna and Muralidar (1968) as given in Figures 2.

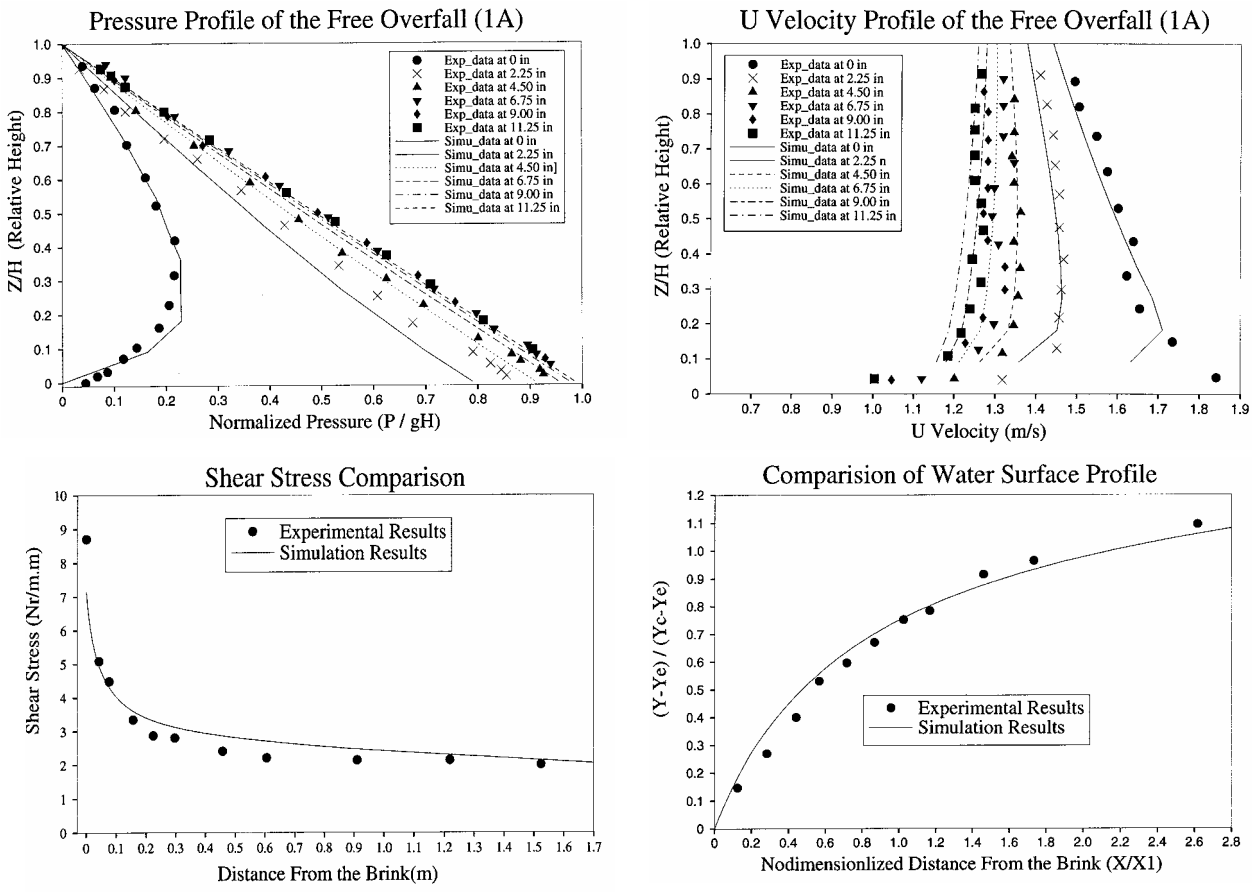

Figure 2. Comparisons of simulated pressure (a), velocity distribution (b), shear stress (c) and free surface profile (d).

Figure 2a shows comparisons of the computed and measured pressure. It can be seen that the pressure distribution is hydrostatic in the region far upstream of the singularity (the brink) and changes gradually to non-hydrostatic pressure in the region close to the brink, and finally to a constant or atmospheric pressure, downstream of the brink. In the upstream of the brink pressure is linearly distributed in vertical direction. However, near the brink, the pressure rapidly changes to parabolic and it gradually vanishes further downstream. The agreement appears to be very good. Figure 2b shows the computed and the measured horizontal velocities. The overall agreement is good except near the brink where the differences may be attributed to the singularity. One should note that near the brink the actual flow may oscillate in time and aeration may take place. As a result, the assumptions made in prescribing boundary conditions over the solid surface near the brink may be unrealistic. For example, the validity of the Law of the Wall may be questionable and the pressure boundary condition $\partial^2 p/\partial z^2=0$ may not be accurate enough. Of course, if the discrepancy is important, the model user should refine the grid locally to enhance the accuracy of the numerical solution near the singularity. Figure 2c and 2d show comparisons of shear stress and water surface profile, respectively. The comparisons indicate the simulation results are quite good.

180° U-shaped Channel Flow

Some distinctive characteristics have been observed in the free surface flows in curved channels such as natural river and streams, irrigation canals, aqueducts, laboratory flumes, etc. In these flows, surface superelevations are observed along the concave or outer bank of channel bends; the flow perpendicular to the channel near the free surface is toward the concave bank and that near the channel bed is moving in the opposite direction. The resulting flow is a helical secondary current combined with the primary flow in the longitudinal direction along the channel. Often times, more than one helical secondary current have been observed, with smaller secondary helical motions occurring in the upper corner of the outer bank. Secondary currents cause a unique morphological evolution of the channel cross-section shape and outer bank migration of meandering rivers. Investigations of these complex three-dimensional flow and morphodynamic processes are needed in soil conservation, river stabilization and restoration/rehabilitation, waterway infrastructure, ecological and environmental research and engineering. The applications of numerical simulation to the studies of the curved channel flows have been emphasized more and more in recent years.

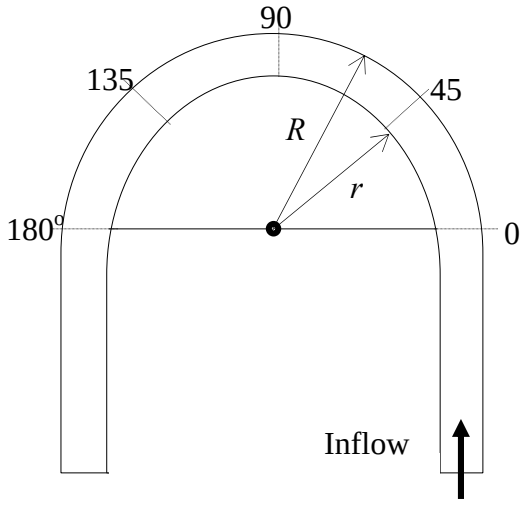

Table 2. Flow condition of the 180° U-shaped channel

Bed slope So	Discharge *Q*(m^3/s)	Depth (m)	Width (m)	Channel Length (m)	Inner Radius r(m)	Outer radius *R*(m)
0.0	0.18	0.20	1.7	25.35	2.9	5.6

Figure 3. Configuration sketch of the physical experiment.

In order to insure quality of a computational simulation model selected for the study of the flows in curved channels, its capability of predicting the aforementioned physical characteristics has to be confirmed. The validation case presented here is the one based on the laboratory experiments

of De Vriend (1979). This case can be utilized to confirm a model's capability in predicting complex three-dimensional flow mechanisms in general, especially in predicting the forming and diminishing of the secondary currents in free surface flows.

The configuration sketch of the physical model is shown in Figure 3, and the flow condition of the experiment is listed in Table 2. The bed and vertical walls were of concrete surface, some thin iron plates that strengthening out bank glass panels were roughened with fine grains (0.006m) to compensate the roughness.

Velocity data were measured in 21 cross-sections including 13 sections in the curved part of the channel, which were equally spaced at 15° interval from 0° to 180°. Six more sections in the downstream straight channel at one meter interval and two other sections were measured in the upstream straight segment, one was 1 meter and the other was 4 meter upstream of the first curved channel section (at 0°). At each of the cross-sections measurements were made along 11 vertical lines and on each vertical line, there were 9 measuring points. The total number of points is therefore 2079 (21x11x9).

Jia and Wang (1992) simulated this case with a zero equation turbulence closure scheme. The finite element mesh was designed to have 49, 15 and 7 sections along longitudinal, transversal and vertical directions, 5145 nodes, respectively. Comparisons of the simulated and measured longitudinal and transversal velocity components show that for engineering purposes the agreements are quite acceptable. The longitudinal and transverse velocity distributions were reproduced reasonably, even though it appears that the discrepancies of velocity components, especially near the side walls and the bed in the channel bend are more pronounced than those of the longitudinal components. A discrepancy one should pointed out is that the vertical profiles of simulated longitudinal velocity components show that the maximum value along each vertical is always at the free surface. This is different from the measurements, in which the maximum is mostly beneath the free surface, especially near the side walls where the maximum can even be in the lower half of the water depth. The transversal velocity components are essentially zero in the straight reach up to the 0° cross-section, where the flow is entering the bend; they are increasing in magnitude quickly near the bend entrance and have a maximum in the vicinity of the apex of the channel (90°); and are gradually decreasing further downstream. The transverse velocity remains in the straight reach (3 meters from the exit of the bend).

The small vortex at the upper comer near the outer bank could not be reproduced by the numerical model. These numerical errors are insignificant in engineering applications, like in most of the published papers reporting computational simulations, because the most important characteristics of a curved channel flow have been predicted correctly. It was found later that this problem can be improved by implementing the nonlinear k-ε turbulence closure to replace the zero equation model for the flow in the channel bend. The simulation of a more realistic curved channel flow using nonlinear k-ε closure and a mush finer mesh (59x97x41=234643) was reported by Jia, et al (2001). By an enhancement of the turbulence closure scheme, the results of their simulation of flows in the same channel and another curved channel with eroded bed were reported and these discrepancies have been significantly reduced. Figure 4 shows the measured and simulated secondary current, one can see that the small vortex at the upper corner of the outer bank (right hand side) has been captured by the improved turbulence closure model. These results indicated that the validation test can be applied to reveal the deficiency of a numerical model, so that the model can be improved before it is applied to real-life problems.

Figure 5 shows comparisons of computed and measured secondary velocity in 45°, 90° and 135° sections.

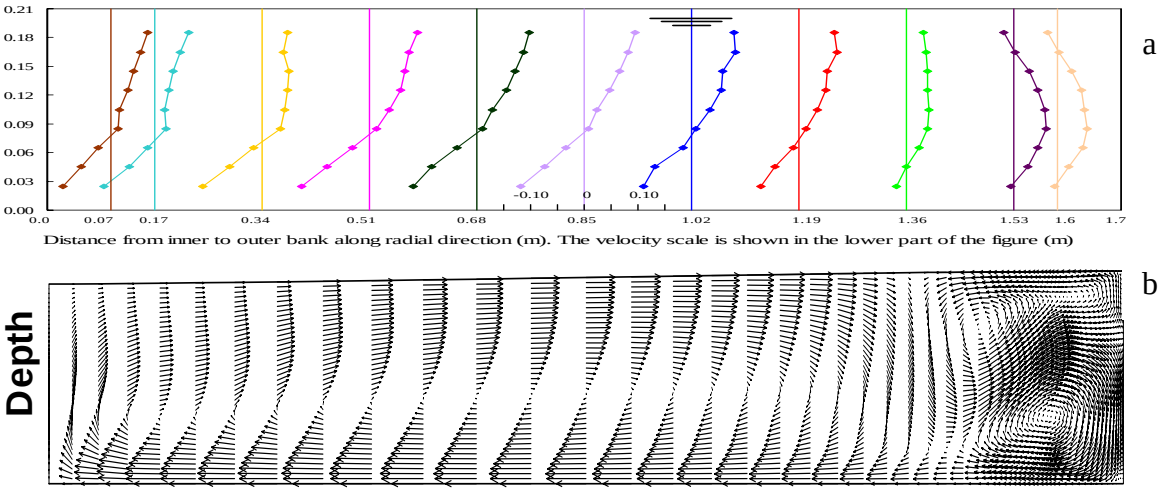

Figure 4 Comparison of measured transverse velocity distribution in 90° section (a) and simulated velocity in the same section.

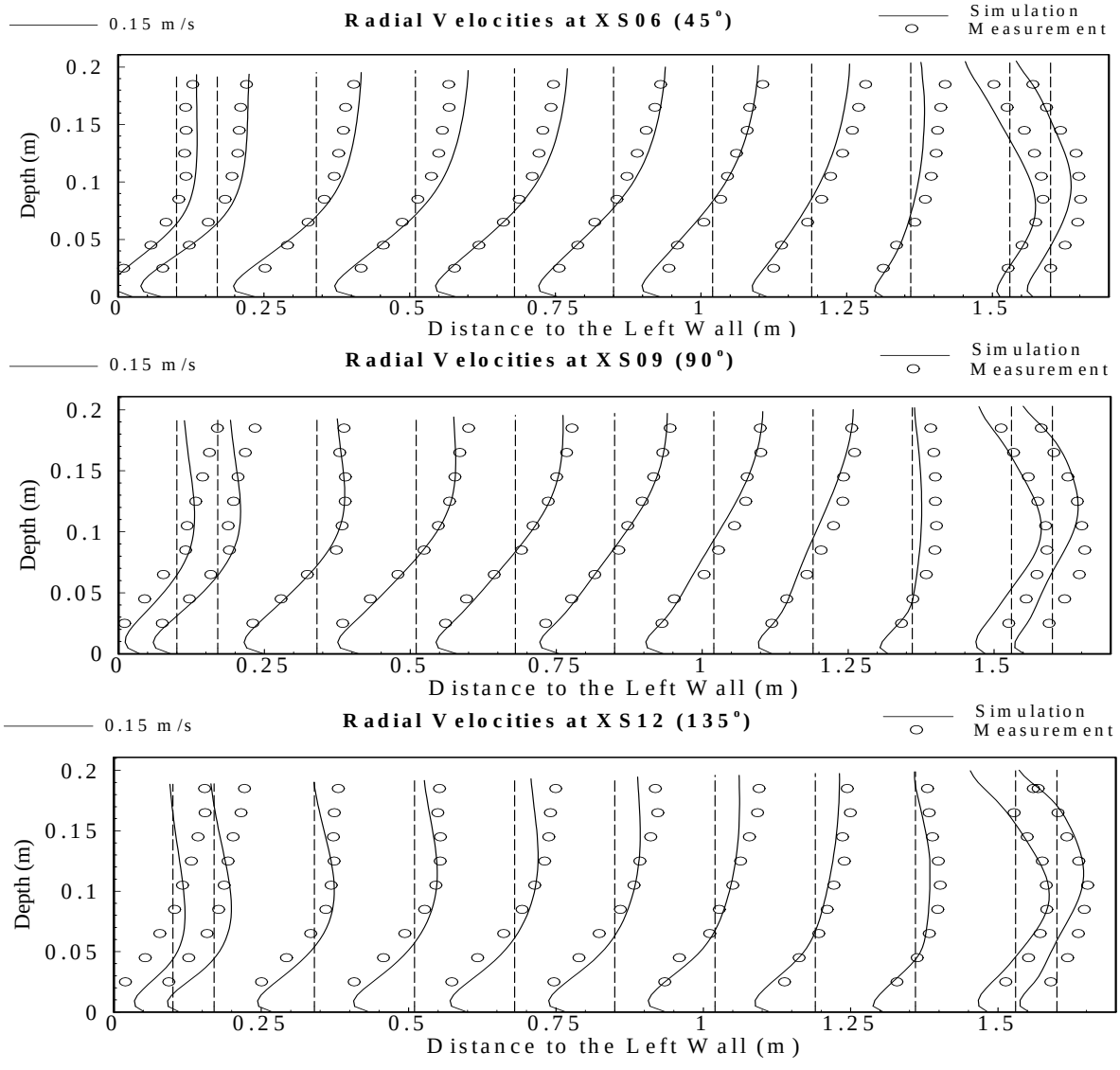

Submerged Weir And Near Field Channel Flow

Since the helical currents in a curved channel bend tend to push the flow toward the concave (outer) bank, it creates problems for channel navigation. Submerged weirs have been installed in channel bendways to improve the flow condition and the channel navigability. Numerical simulations were conducted to analyze the near field flow pattern and study the optimal weir parameters for channel navigation. In addition, one would have higher confidence to apply the model to a field study if it is fully verified with the physical model data. Model validation was performed based on flow data measured during the a physical model study conducted at Coastal and Hydraulic Laboratory of ERDC, US Army Corps of Engineers, Waterways Experimental Station, Vicksburg, Mississippi. The channel plan form, cross sectional form, and the location of the submerged weir and the simulation domains are shown in Figure 6. The length of the channel center line is more then 70 meters and the width of the channel (water surface) is about 3.2 meters.

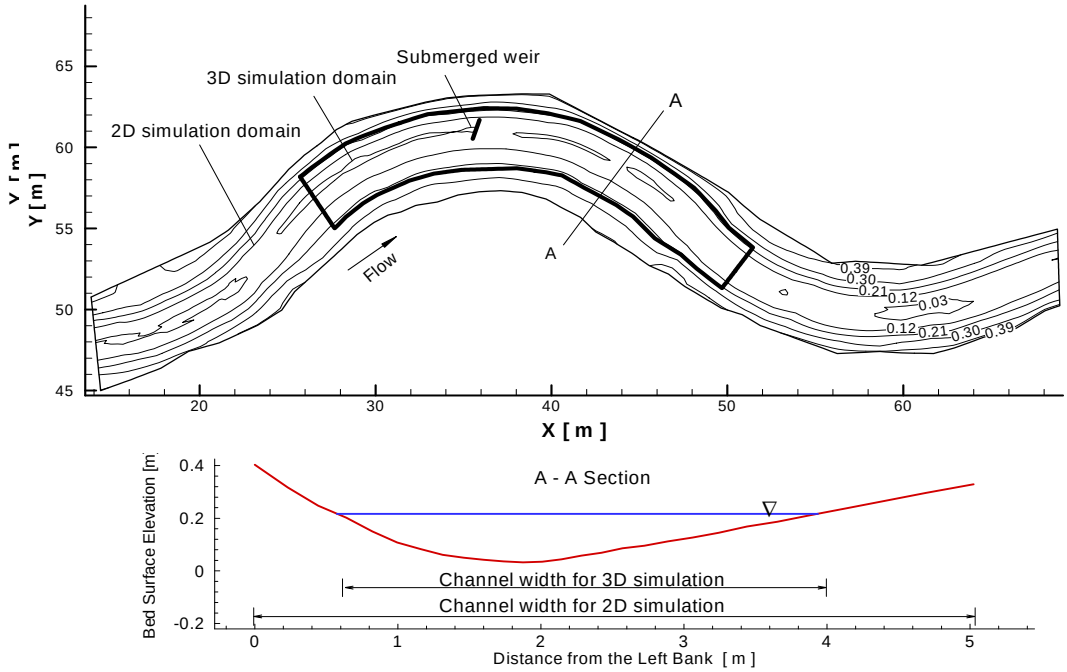

Figure 6. Physical model set up and numerical simulation domain.

The submerged weir of α= 20^o and L= 1.8m is clearly seen. The dot lines aligned parallel to the weir are measurement ranges. They are numbered from upstream to downstream, with three ranges on the front side (upstream) and the remaining on the back or downstream side. The longitudinal spacing between the first and the second range, the third and forth, and between the seventh and those that follow were 0.3048 m. The spacing between the other ranges are 0.1524m. The transversal spacing of points along range 1, 8, 9, and 10 is 0.3048 m, with a spacing of 0.1524m for the rest of ranges. Velocity data were taken at three levels (0.2 h, 0.6 h from surface and close to bed) at each measuring location. The

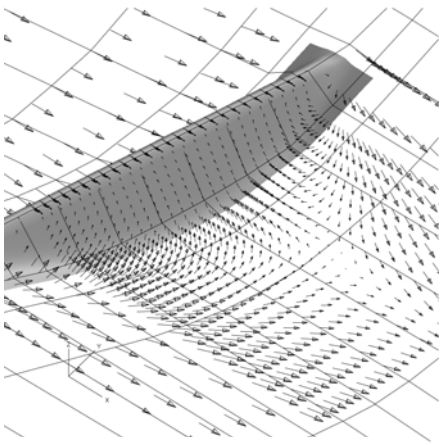

Figure 7. Near field flow pattern around the weir and mesh distribution

mesh used for this simulation has been refined in the vicinity of the weir and close to the weir and bed surface. Figure 7 shows near bed mesh distribution (coarsened flow clarity) and computed near bed velocity vectors using CCHE3D (Jia et al, 2005).

Figure 8 shows computed and measured velocity magnitude along the 10 measurement ranges (sections). The velocities shown were measured at 20% and 60% of local flow depth (0.2 *h and 0.6 h*) from the water surface. The horizontal axes are the distance from the left (outer) bank of the channel. The comparison of simulation and measurements for Run1 showed similar agreement in trend.

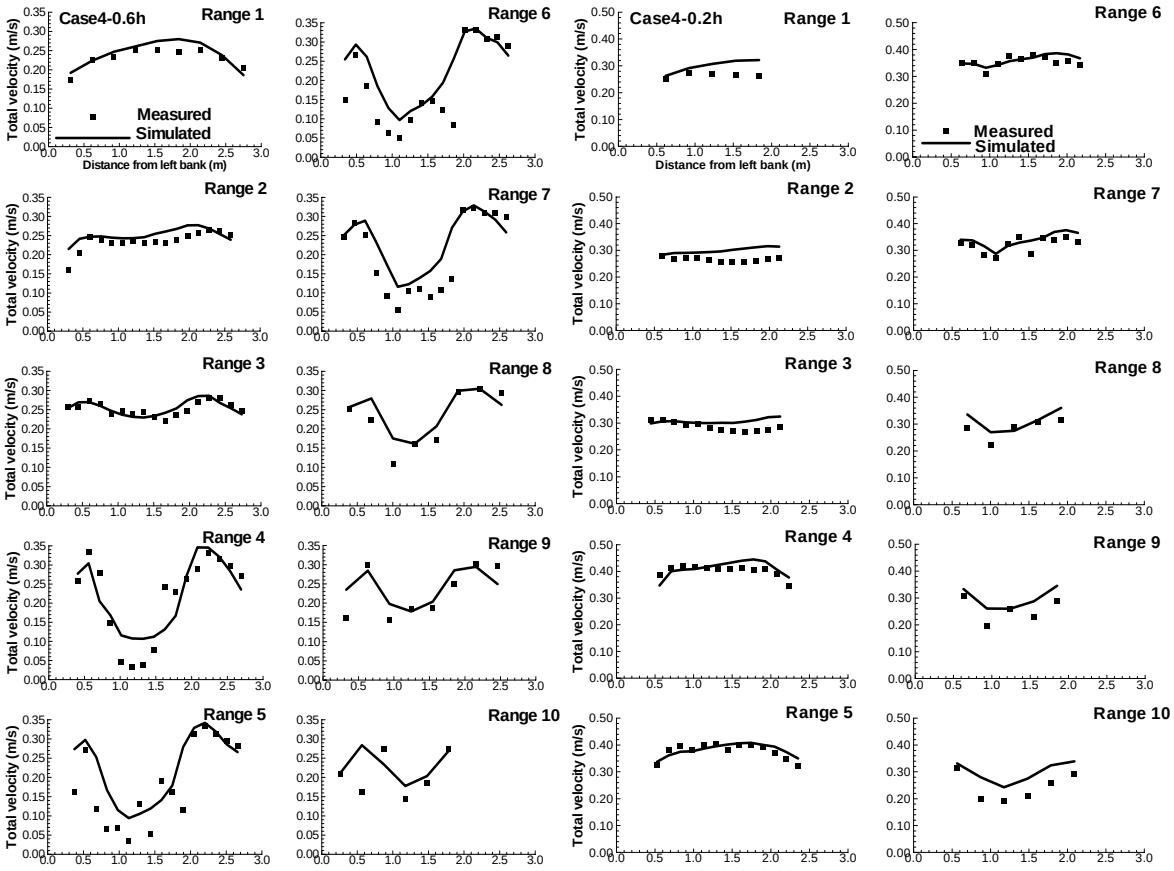

Figure 8. Comparison of measured computed velocity profiles around a submerged weir

The general trend of agreement between the measurement and model simulation results are very good. The flow approaching to the weir from upstream slows down in the center of the channel but accelerates near banks; a triangular shaped recirculation zone was formed behind the weir in which the near bed flow moves backward. More importantly, the flow across the weir is redirected to be perpendicular to the weir and against the general helical flow direction. This flow pattern disturbed the helical current distribution mainly in downstream of the weir.

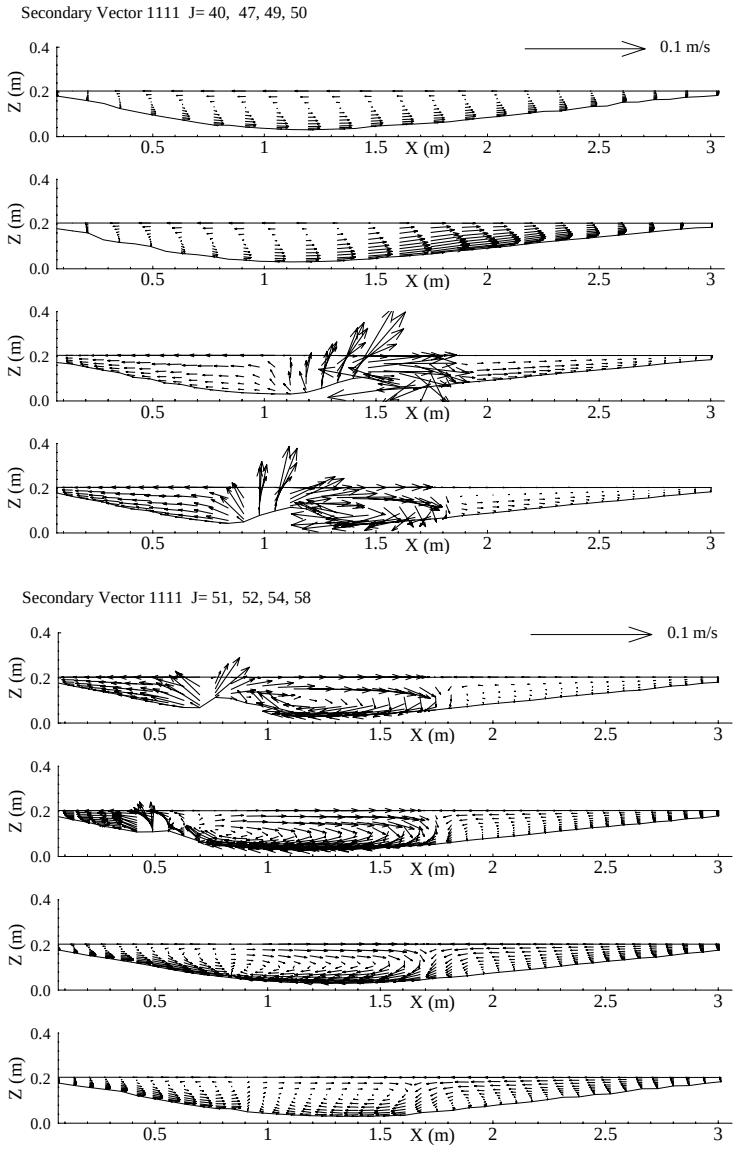

Figure 9 Predicted Secondary Current Near a Submerged Weir

Figure 9 shows the secondary current in the vicinity of the weir. The general helical current is formed in the channel approaching to the weir, it starts changing when the weir is close. Inverse secondary current is created near and behind the weir, it persists for a distance downstream and gradually reduces its intensity due to dissipation and channel curvature. This distance is the range in which tow-boat navigation would be improved because the near surface flow may force it toward the inner bank.

The validated model was also applied to simulating flow with a weir field in a real world situation: Victoria Bendway, Mississippi River. The simulation was validated with field data and indicated that the weirs installed in the Victoria Bendway improved the flow condition to certain extent. Not all the weirs, however, perform at the same level.

CONCLUSION

Numerical model validation using physical model data is a key step to confirm if a particular model is capable of reproducing true physical processes and mechanism. It can be applied to study real

world problems only after the model is validated. *Physical Validations* should be carried out when a new mechanism in an application is concerned.

Test cases presented in this paper, free overfall, 180° curved channel, and channel with a submerged weir, indicated the importance of capabilities such as dynamic pressure, free surface, and turbulence closure schemes. CCHE3D was used to demonstrate these test cases and the validation objectives.

ACKNOWLEDGEMENT

This work is a result of research supported in part by the USDA Agriculture Research Service under Specific Research Agreement No. 58-6408-7-035 (monitored by the USDA-ARS National Sedimentation Laboratory)

REFERENCES

De Vriend, D.J., 1979, *Flow measurements in a Curved Rectangular Channel,* Laboratory of Fluid Mechanics, Department of Civil Engineering, Delft University of Technology, Internal Report No. 9-79.

Jia, Y., and Wang, S.S.Y., 1992, "Computational model verification test case using flume data". Hydraulic Engineering, pp436-441, ASCE.

Jia, Y., Kitamura, T., and Wang, S.S.Y., 2001, “Simulation scour process in a plunge pool with loose material”, ASCE, *Journal of Hydraulic Engineering*, Vol. 127, No. 3, pp219-229.

Jia, Y., Blanckaert, K., and Wang, S.S.Y., 2001, "Simulation of secondary flow in curved channels". Published on the FMTM2001 International Conference, Tokyo, Japan.

Jia, Y., Scott, S., Xu, Y.C., Huang, S.L., and Wang, S.S.Y., 2005, “Three-Dimensional Numerical Simulation and Analysis of Flows around a Submerged Weir in a Channel Bendway”, *Journal of Hydraulic Engineering*, Vol. 131, No. 8:682-693, August 1, 2005.

Marchi, E., 1993, “On the free overfall”, *Journal of Hydraulic Research*, Vol. 31, No. 6, pp777-790, Vol. 32, No.5, pp 792,796.

Rajaratnam, N., and Muralidhar, D., 1968, “Characteristics of the rectangular free over fall”, *Journal of Hydraulic Research*, Vol. 6, No. 3, pp233-258.

Rouse, H., 1936, “Discharge characters of the free overfall”, *Civil Engineering*, Vol. 6, No. 4, pp 257-260.

Strelkoff, T., and Moayeri. M., 1970, “Pattern of potential flow in a free overfall”, ASCE, *Journal of Hydraulic Division*, Vol. 96, No. HY4, pp 879-901.